

# A time adaptive multirate Dirichlet–Neumann waveform relaxation method for heterogeneous coupled heat equations

Peter Meisrimel<sup>1</sup>, Azahar Monge<sup>1,2</sup>, Philipp Birken<sup>1</sup>

November 28, 2021

<sup>1</sup>*Centre for the mathematical sciences, Numerical Analysis, Lund University, Lund, Sweden  
email: peter.meisrimel@na.lu.se, azahar.sz@gmail.com, philipp.birken@na.lu.se*

<sup>2</sup>*Chair of Computational Mathematics, University of Deusto, Spain, Bilbao*

## Abstract

We consider partitioned time integration for heterogeneous coupled heat equations. First and second order multirate, as well as time-adaptive Dirichlet-Neumann Waveform relaxation (DNWR) methods are derived. In 1D and for implicit Euler time integration, we analytically determine optimal relaxation parameters for the fully discrete scheme.

We test the robustness of the relaxation parameters on the second order multirate method in 2D. DNWR is shown to be very robust and consistently yielding fast convergence rates, whereas the closely related Neumann-Neumann Waveform relaxation (NNWR) method is slower or even diverges.

The waveform approach naturally allows for different timesteps in the subproblems. In a performance comparison for DNWR, the time-adaptive method dominates the multirate method due to automatically finding suitable stepsize ratios. Overall, we obtain a fast, robust, multirate and time adaptive partitioned solver for unsteady conjugate heat transfer.

**Keywords:** *Thermal Fluid-Structure Interaction, Coupled Problems, Dirichlet–Neumann Method, Multirate, Time Adaptivity, Waveform Relaxation*

**Mathematics Subject Classification (2000):** *80M10, 35Q79, 65M22, 65F99*

This research is supported by the Swedish e-Science collaboration eSENCE, which we gratefully acknowledge.

## 1 Introduction

We consider efficient numerical methods for the partitioned time integration of coupled multi-physics problems. In a partitioned approach different codes for the sub-problems are reused and the coupling is done by a coupling code which calls interface functions of the segregated codes [9, 10]. These algorithms are currently an active research topic driven by certain multiphysics applications where multiple physical models or multiple simultaneous physical phenomena involve solving coupled systems of partial differential equations (PDEs).

An example of this is fluid structure interaction (FSI) [39, 7]. Our prime motivation is thermal interaction between fluids and structures, also called conjugate heat transfer. There are two domains with jumps in the material coefficients across the connecting interface. Conjugate heat transfer plays an important role in many applications and its simulation has proved essential [2]. Examples for thermal fluid structure interaction are cooling of gas-turbine blades, thermal anti-icing systems of airplanes [8], supersonic reentry of vehicles from space [27, 19], gas quenching, which is an industrial heat treatment of metal workpieces [18, 37] or the cooling of rocket nozzles [21, 22].

The most common form of coupling is a Dirichlet-Neumann (DN) approach, in which one problem has a Dirichlet boundary condition on the shared interface, while the other one uses a

Neumann boundary condition. In the iteration, they provide each other with the suitable boundary data, i.e. a flux or the interface value. Thus, there is a connection to Domain Decomposition methods.

From the partitioned time integration, we require that it allows for variable and adaptive time steps, preserves the order of the time integration in the subsolvers, and it should be robust and fast. A technique that promises to deliver these properties is the so called Waveform relaxation (WR). An iteration requires solving the subproblems on a time window. Thereby, continuous interface functions, obtained via suitable interpolation, are provided from the respective other problem. WR methods were originally introduced by [24] for ordinary differential equation (ODE) systems, and used for the first time to solve time dependent PDEs in [14, 15]. They allow the use of different spatial and time discretizations for each subdomain. This is especially useful in problems with strong jumps in the material coefficients [12] or the coupling of different models for the subdomains [11].

A key problem is to make the Waveform iteration fast. A black box approach is to make use of Quasi-Newton methods, leading to Quasi-Newton Waveform iterations [35]. Here, we follow instead the idea to tailor very fast methods to a specific problem. In particular, we consider the Neumann-Neumann Waveform relaxation (NNWR) and Dirichlet-Neumann Waveform relaxation (DNWR) method of Gander et al. [23, 13], which are WR methods based on the classical Neumann-Neumann and Dirichlet-Neumann iterations. The DNWR method is serial, whereas with NNWR, one can solve the subproblems in parallel. Using an optimal relaxation parameter, convergence in two iterations is obtained for the continuous iteration in 1D. In [31], a fully discrete multirate NNWR method for heterogeneous coupled heat equations is presented. Optimal relaxation parameters are determined for the 1D case. The method was extended to the time adaptive case in [33].

However, the NNWR method is extremely sensitive to the choice of the relaxation parameter, leading to a lack of robustness. In this paper, we therefore focus on the DNWR method, see also [32]. The standard DN method was known to be a very fast method for thermal interaction between air and steel [6, 5, 3]. This was thoroughly analyzed for the fully discrete case for two coupled heat equations with different material properties in [30] and for coupled Laplace equations in [16]. Thus, we can expect the waveform variant to be a fast solver not only when using an optimal relaxation parameter. The technique employed here to determine optimal relaxation parameters follows [31], which considers the fully discrete iteration for a 1D model problem. Then, using the Toeplitz structure of the arising matrices, a formula for the spectral radius of the iteration matrix can be found and the optimal relaxation parameter can be analytically determined.

We present first and second order multirate WR methods, as well as a second order time adaptive method. The time integration methods we use as a base are implicit Euler and a second order singly diagonally implicit Runge-Kutta (SDIRK2) method. The optimal relaxation parameter  $\Theta_{opt}$  from the analysis of 1D and implicit Euler yields good results for 2D and SDIRK2. We show how to adapt  $\Theta_{opt}$  for use in the multirate and time-adaptive setting to get good convergence rates. Additionally, we experimentally show that the convergence results also extend to non-square geometries. Overall, our DNWR method yields a fast and robust solver for unsteady conjugate heat transfer.

## 2 Model problem

The unsteady transmission problem reads as follows, where we consider a domain  $\Omega \subset \mathbb{R}^d$  which is cut into two subdomains  $\Omega = \Omega_1 \cup \Omega_2$  with transmission conditions at the interface  $\Gamma = \partial\Omega_1 \cap \partial\Omega_2$ :

$$\begin{aligned} \alpha_m \frac{\partial u_m(\mathbf{x}, t)}{\partial t} - \nabla \cdot (\lambda_m \nabla u_m(\mathbf{x}, t)) &= 0, \quad (\mathbf{x}, t) \in \Omega_m \times (0, T_f], \quad m = 1, 2, \\ u_m(\mathbf{x}, t) &= 0, \quad (\mathbf{x}, t) \in \partial\Omega_m \setminus \Gamma \times [0, T_f], \\ u_1(\mathbf{x}, t) &= u_2(\mathbf{x}, t), \quad (\mathbf{x}, t) \in \Gamma \times (0, T_f], \\ \lambda_2 \frac{\partial u_2(\mathbf{x}, t)}{\partial \mathbf{n}_2} &= -\lambda_1 \frac{\partial u_1(\mathbf{x}, t)}{\partial \mathbf{n}_1}, \quad (\mathbf{x}, t) \in \Gamma \times (0, T_f], \\ u_m(\mathbf{x}, 0) &= u_m^0(\mathbf{x}), \quad \mathbf{x} \in \Omega_m, \end{aligned} \quad (1)$$

where  $\mathbf{n}_m$  is the outward normal to  $\Omega_m$  for  $m = 1, 2$ .

The constants  $\lambda_1$  and  $\lambda_2$  describe the thermal conductivities of the materials on  $\Omega_1$  and  $\Omega_2$  respectively.  $D_1$  and  $D_2$  represent the thermal diffusivities of the materials and are defined by

$$D_m = \lambda_m / \alpha_m, \quad \text{with} \quad \alpha_m = \rho_m c_{p_m},$$

where  $\rho_m$  is the density and  $c_{p_m}$  the specific heat capacity of the material placed in  $\Omega_m$ ,  $m = 1, 2$ .

## 3 The Dirichlet-Neumann Waveform Relaxation algorithm

The Dirichlet-Neumann Waveform relaxation (DNWR) method is inspired by substructuring methods from Domain Decomposition. The PDEs are solved sequentially using a Dirichlet-respectively Neumann boundary condition with data given from the solution of the other problem, c.f. [25, 26].

Given an interface solution  $g^{(k)}(\mathbf{x}, t)$ ,  $(\mathbf{x}, t) \in \Gamma \times [0, T_f]$ , it consists of the following three-step iteration. Imposing continuity of the solution across the interface, one first finds the local solution  $u_1^{(k+1)}(\mathbf{x}, t)$  on  $(\mathbf{x}, t) \in \Omega_1 \times [0, T_f]$  by solving the Dirichlet problem:

$$\begin{aligned} \alpha_1 \frac{\partial u_1^{(k+1)}(\mathbf{x}, t)}{\partial t} - \nabla \cdot (\lambda_1 \nabla u_1^{(k+1)}(\mathbf{x}, t)) &= 0, \quad (\mathbf{x}, t) \in \Omega_1 \times (0, T_f], \\ u_1^{(k+1)}(\mathbf{x}, t) &= 0, \quad (\mathbf{x}, t) \in \partial\Omega_1 \setminus \Gamma \times [0, T_f], \\ u_1^{(k+1)}(\mathbf{x}, t) &= g^{(k)}(\mathbf{x}, t), \quad (\mathbf{x}, t) \in \Gamma \times [0, T_f], \\ u_1^{(k+1)}(\mathbf{x}, 0) &= u_1^0(\mathbf{x}), \quad \mathbf{x} \in \Omega_1. \end{aligned} \quad (2)$$

The typical initial guess is  $g^{(0)}(\mathbf{x}, t) = u(\mathbf{x}, 0)|_{\Gamma}$ , i.e., extrapolation of the interface initial value.

Then, imposing continuity of the heat fluxes across the interface, one finds the local solution  $u_2^{(k+1)}(\mathbf{x}, t)$  on  $\Omega_2$  by solving the Neumann problem:

$$\begin{aligned} \alpha_2 \frac{\partial u_2^{(k+1)}(\mathbf{x}, t)}{\partial t} - \nabla \cdot (\lambda_2 \nabla u_2^{(k+1)}(\mathbf{x}, t)) &= 0, \quad (\mathbf{x}, t) \in \Omega_2 \times (0, T_f], \\ u_2^{(k+1)}(\mathbf{x}, t) &= 0, \quad (\mathbf{x}, t) \in \partial\Omega_2 \setminus \Gamma \times [0, T_f], \\ \lambda_2 \frac{\partial u_2^{(k+1)}(\mathbf{x}, t)}{\partial \mathbf{n}_2} &= -\lambda_1 \frac{\partial u_1^{(k+1)}(\mathbf{x}, t)}{\partial \mathbf{n}_1}, \quad (\mathbf{x}, t) \in \Gamma \times [0, T_f], \\ u_2^{(k+1)}(\mathbf{x}, 0) &= u_2^0(\mathbf{x}), \quad \mathbf{x} \in \Omega_2. \end{aligned} \quad (3)$$

Finally, the interface values are updated with

$$g^{(k+1)}(\mathbf{x}, t) = \Theta u_2^{(k+1)}(\mathbf{x}, t) + (1 - \Theta) g^{(k)}(\mathbf{x}, t), \quad (\mathbf{x}, t) \in \Gamma \times [0, T_f], \quad (4)$$

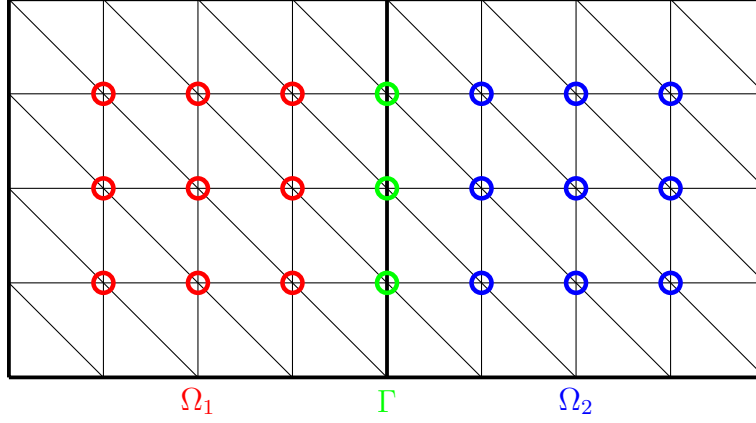


Figure 1: Splitting of  $\Omega$  and finite element triangulation.

where  $\Theta \in (0, 1]$  is the relaxation parameter. Note that choosing an appropriate relaxation parameter is crucial to get a fast convergence rate. In [13], the optimal relaxation parameter in 1D has been proven to be  $\Theta = 1/2$  for  $\lambda_1 = \lambda_2 = \alpha_1 = \alpha_2 = 1$  and subdomains of equal size. If one uses the optimal relaxation parameter, two iterations are enough for subdomains of equal size.

## 4 Semidiscrete method

We now describe a rather general space discretization of (2)-(4). The core property we need is that the meshes of  $\Omega_1$  and  $\Omega_2$  share the same nodes on  $\Gamma$  as shown in Figure 1. Furthermore, we assume that there is a specific set of unknowns associated with the interface nodes. Otherwise, we allow at this point for arbitrary meshes on both sides. Then, letting  $\mathbf{u}_I^{(m)} : [0, T_f] \rightarrow \mathbb{R}^{R_m}$  where  $R_m$  is the number of grid points on  $\Omega_m$ ,  $m = 1, 2$ , and  $\mathbf{u}_\Gamma : [0, T_f] \rightarrow \mathbb{R}^s$ , where  $s$  is the number of grid points at the interface  $\Gamma$ , we can write a general discretization of the first two equations in (2) and (3), respectively, in a compact form as:

$$\mathbf{M}_{II}^{(1)} \dot{\mathbf{u}}_I^{(1),(k+1)}(t) + \mathbf{A}_{II}^{(1)} \mathbf{u}_I^{(1),(k+1)}(t) = -\mathbf{M}_{I\Gamma}^{(1)} \dot{\mathbf{u}}_\Gamma^{(k)}(t) - \mathbf{A}_{I\Gamma}^{(1)} \mathbf{u}_\Gamma^{(k)}(t), \quad t \in [0, T_f], \quad (5)$$

$$\mathbf{M}_{II}^{(2)} \dot{\mathbf{u}}_I^{(2),(k+1)}(t) + \mathbf{A}_{II}^{(2)} \mathbf{u}_I^{(2),(k+1)}(t) + \mathbf{M}_{I\Gamma}^{(2)} \dot{\mathbf{u}}_\Gamma^{(k+1)}(t) + \mathbf{A}_{I\Gamma}^{(2)} \mathbf{u}_\Gamma^{(k+1)}(t) = \mathbf{0}, \quad t \in [0, T_f], \quad (6)$$

with initial conditions  $\mathbf{u}_I^{(m)}(0) \in \mathbb{R}^{S_m}$  resp.  $\mathbf{u}_\Gamma(0) \in \mathbb{R}^s$ ,  $m = 1, 2$ .

To close the system, we need an approximation of the normal derivatives on  $\Gamma$ . Letting  $\phi_j$  be a nodal FE basis function on  $\Omega_m$  for a node on  $\Gamma$  we observe that the normal derivative of  $u_m$  with respect to the interface can be written as a linear functional using Green's formula [38, pp. 3]. Thus, the approximation of the normal derivative is given by

$$\begin{aligned} \lambda_m \int_\Gamma \frac{\partial u_m(\mathbf{x}, t)}{\partial \mathbf{n}_m} \phi_j(\mathbf{x}) dS &= \lambda_m \int_{\Omega_m} (\Delta u_m(\mathbf{x}, t) \phi_j(\mathbf{x}) + \nabla u_m(\mathbf{x}, t) \nabla \phi_j(\mathbf{x})) d\mathbf{x} \\ &= \alpha_m \int_{\Omega_m} \frac{d}{dt} u_m(\mathbf{x}, t) \phi_j(\mathbf{x}) d\mathbf{x} + \lambda_m \int_{\Omega_m} \nabla u_m(\mathbf{x}, t) \nabla \phi_j(\mathbf{x}) d\mathbf{x}, \quad t \in [0, T_f], \quad m = 1, 2. \end{aligned}$$

Consequently, the equation

$$\begin{aligned} &\mathbf{M}_{II}^{(2)} \dot{\mathbf{u}}_I^{(2),(k+1)}(t) + \mathbf{A}_{II}^{(2)} \mathbf{u}_I^{(2),(k+1)}(t) + \mathbf{M}_{I\Gamma}^{(2)} \dot{\mathbf{u}}_\Gamma^{(k+1)}(t) + \mathbf{A}_{I\Gamma}^{(2)} \mathbf{u}_\Gamma^{(k+1)}(t) \\ &= - \left( \mathbf{M}_{I\Gamma}^{(1)} \dot{\mathbf{u}}_\Gamma^{(1),(k+1)}(t) + \mathbf{A}_{I\Gamma}^{(1)} \mathbf{u}_\Gamma^{(1),(k+1)}(t) + \mathbf{M}_{I\Gamma}^{(1)} \dot{\mathbf{u}}_\Gamma^{(k)}(t) + \mathbf{A}_{I\Gamma}^{(1)} \mathbf{u}_\Gamma^{(k)}(t) \right), \quad t \in [0, T_f], \end{aligned} \quad (7)$$

is a semi-discrete version of the third equation in (3) and completes the system (5)-(6).

Omitting the iteration indices, the system of IVPs defined by (5), (6) and (7) is a semidiscretization of (1). We refer to it as the (semidiscrete) monolithic system and its solution as the monolithic solution.

Then, the semidiscrete DNWR algorithm is as follows: In each iteration  $k$ , one first solves the Dirichlet problem (5), obtaining  $\mathbf{u}_I^{(1),(k+1)}$ . Then, using the function of unknowns  $\mathbf{u}^{(k+1)} = \left( \mathbf{u}_I^{(2),(k+1)T} \mathbf{u}_\Gamma^{(k+1)T} \right)^T$ , one solves the following Neumann problem that corresponds to equations (6) and (7):

$$\mathbf{M}\dot{\mathbf{u}}^{(k+1)}(t) + \mathbf{A}\mathbf{u}^{(k+1)}(t) = \mathbf{b}^{(k)}(t), \quad t \in [0, T_f], \quad \mathbf{u}(0) = \mathbf{u}_0, \quad (8)$$

where

$$\mathbf{M} = \begin{pmatrix} \mathbf{M}_{II}^{(2)} & \mathbf{M}_{I\Gamma}^{(2)} \\ \mathbf{M}_{\Gamma I}^{(2)} & \mathbf{M}_{\Gamma\Gamma}^{(2)} \end{pmatrix}, \quad \mathbf{A} = \begin{pmatrix} \mathbf{A}_{II}^{(2)} & \mathbf{A}_{I\Gamma}^{(2)} \\ \mathbf{A}_{\Gamma I}^{(2)} & \mathbf{A}_{\Gamma\Gamma}^{(2)} \end{pmatrix}, \quad \mathbf{b}^{(k)}(t) = \begin{pmatrix} \mathbf{0} \\ -\mathbf{q}^{(k+1)}(t) \end{pmatrix},$$

with the heat flux

$$\mathbf{q}^{(k+1)}(t) = \mathbf{M}_{\Gamma I}^{(1)} \dot{\mathbf{u}}_I^{(1),(k+1)}(t) + \mathbf{A}_{\Gamma I}^{(1)} \mathbf{u}_I^{(1),(k+1)}(t) + \mathbf{M}_{\Gamma\Gamma}^{(1)} \dot{\mathbf{u}}_\Gamma^{(k)}(t) + \mathbf{A}_{\Gamma\Gamma}^{(1)} \mathbf{u}_\Gamma^{(k)}(t). \quad (9)$$

Finally, the interface solutions are updated by

$$\mathbf{u}_\Gamma^{(k+1)} \leftarrow \Theta \mathbf{u}_\Gamma^{(k+1)} + (1 - \Theta) \mathbf{u}_\Gamma^{(k)}. \quad (10)$$

The iteration starts with a function initial guess  $\mathbf{u}_\Gamma^{(0)}$ , we use  $\mathbf{u}_\Gamma^{(0)} \equiv \mathbf{u}_\Gamma(0)$ . Since the iteration is done on functions, one would like to terminate when  $\|\mathbf{u}_\Gamma^{(k+1)} - \mathbf{u}_\Gamma^{(k)}\| \leq \text{TOL}_{WR}$  is met, where  $\text{TOL}_{WR}$  is a user defined tolerance. Since we expect the time integration error to grow with  $t$ , we only compare the update at  $T_f$ . Our termination criterion is

$$\|\mathbf{u}_\Gamma^{(k+1)}(T_f) - \mathbf{u}_\Gamma^{(k)}(T_f)\|_\Gamma \leq \text{TOL}_{WR} \cdot \|\mathbf{u}_\Gamma(0)\|_\Gamma, \quad (11)$$

i.e., the relative update w.r.t. the initial value at the interface. We use the discrete  $\mathcal{L}^2$  interface norm, given by

$$\|\cdot\|_\Gamma = \|\cdot\|_2 \Delta x^{(d-1)/2},$$

for a mesh uniform at the interface. Here,  $d$  is the spatial dimension of (1).

## 5 Multirate time discretization

In the case of non-matching material parameters  $\alpha_m$ ,  $\lambda_m$ , the Dirichlet and the Neumann problems (5) and (8) have different needs for time-discretization. Consequently, we want the possibility to use different time integration methods and different step-sizes on each subdomain. To this end, we first define interpolation functions in time at the interface. We then present two fully discrete DNWR methods, which use the implicit Euler, resp. the second order singly diagonally implicit Runge-Kutta method (SDIRK2) for time integration. We formulate these for general step-sizes  $\Delta t_n$ . One obtains the multirate resp. adaptive algorithm by choosing different step-sizes on the different subdomains.

### 5.1 Interpolation

We denote the fully discrete interface solutions resp. heat fluxes by

$$\underline{\mathbf{u}}_\Gamma^{(k)} := \{\mathbf{u}_\Gamma^{(k),n}\}_{n=0,\dots,N_2^{(k)}} \quad \text{and} \quad \underline{\mathbf{q}}^{(k)} := \{\mathbf{q}^{(k),n}\}_{n=0,\dots,N_1^{(k)}},$$

where  $N_m^{(k)}$  is the number of timesteps on  $\Omega_m$  in the  $k$ -th iteration. We define the interpolants as follows:

$$\mathcal{I}(\underline{\mathbf{u}}_\Gamma^{(k)}) \in \mathcal{C}([0, T_f]; \mathbb{R}^{d_s}) \quad \text{and} \quad \mathcal{I}(\underline{\mathbf{q}}^{(k)}) \in \mathcal{C}([0, T_f]; \mathbb{R}^{d_s}),$$

omitting the dependencies of the interpolants on the time-grids for readability. Now, when deriving the fully discrete DNWR methods, we replace all evaluations of the interface temperatures in the Dirichlet problem (5) by evaluations of the interpolant  $\mathcal{I}(\underline{\mathbf{u}}_\Gamma^{(k)})$ . Analogously, we replace heat flux evaluations for the Neumann problem (8) by evaluations of  $\mathcal{I}(\underline{\mathbf{q}}^{(k+1)})$ .

The interpolation is done by a coupling code, such that a solver for a subdomain need not know about the other time grid. Here, we consider *linear polynomial interpolation*.

For readability, we omit dependencies of the time-points on  $(k)$  in the following derivations. In case of time-grids varying with  $k$ , all time-point evaluations correspond to the time-grid of the current iteration. The time-grid of the previous iteration is only used to define the underlying interpolation data.

## 5.2 Implicit Euler

The implicit Euler method is defined by approximating the derivative term via a standard backward differences. We will use this approximation for derivative terms, i.e.,

$$\begin{aligned} \frac{d}{dt} \mathcal{I}(\underline{\mathbf{u}}_\Gamma^{(k)})(t_{n+1}) &\approx \left( \mathcal{I}(\underline{\mathbf{u}}_\Gamma^{(k)})(t_{n+1}) - \mathcal{I}(\underline{\mathbf{u}}_\Gamma^{(k)})(t_n) \right) / \Delta t_n \\ \text{and} \quad \dot{\mathbf{u}}_I^{(1),(k+1)}(t_{n+1}) &\approx \left( \mathbf{u}_I^{(1),(k+1)}(t_{n+1}) - \mathbf{u}_I^{(1),(k+1)}(t_n) \right) / \Delta t_n. \end{aligned}$$

In each iteration  $k$  of the WR algorithm, given the initial value  $\mathbf{u}_I^{(1),(k+1),0} = \mathbf{u}_I^{(1)}(0)$  and the function  $\mathcal{I}(\underline{\mathbf{u}}_\Gamma^{(k)})(t)$ , we apply the implicit Euler scheme to the Dirichlet problem (5), which yields

$$\begin{aligned} &\left( \mathbf{M}_{II}^{(1)} + \Delta t \mathbf{A}_{II}^{(1)} \right) \mathbf{u}_I^{(1),(k+1),n+1} \\ &= \mathbf{M}_{II}^{(1)} \mathbf{u}_I^{(1),(k+1),n} - \left( \mathbf{M}_{II}^{(1)} + \Delta t_n \mathbf{A}_{II}^{(1)} \right) \mathcal{I}(\underline{\mathbf{u}}_\Gamma^{(k)})(t_{n+1}) + \mathbf{M}_{II}^{(1)} \mathcal{I}(\underline{\mathbf{u}}_\Gamma^{(k)})(t_n), \quad n = 0, \dots, N_1^{(k+1)} - 1. \end{aligned} \quad (12)$$

We compute the discrete heat fluxes as output of the Dirichlet solver by approximating the derivatives in (9) using standard backward differences, this yields

$$\begin{aligned} \mathbf{q}^{(k+1),n+1} &= \left( \mathbf{M}_{\Gamma I}^{(1)} / \Delta t_n + \mathbf{A}_{\Gamma I}^{(1)} \right) \mathbf{u}_I^{(1),(k+1),n+1} - \mathbf{M}_{\Gamma I}^{(1)} / \Delta t_n \mathbf{u}_I^{(1),(k+1),n} \\ &\quad + \left( \mathbf{M}_{\Gamma \Gamma}^{(1)} / \Delta t_n + \mathbf{A}_{\Gamma \Gamma}^{(1)} \right) \mathcal{I}(\underline{\mathbf{u}}_\Gamma^{(k)})(t_{n+1}) - \mathbf{M}_{\Gamma \Gamma}^{(1)} / \Delta t_n \mathcal{I}(\underline{\mathbf{u}}_\Gamma^{(k)})(t_n), \quad n = 0, \dots, N_1^{(k+1)} - 1. \end{aligned} \quad (13)$$

The initial flux  $\mathbf{q}^{(k+1),0}$ , which is required in the interpolation, is analogously computed using standard forward differences to approximate derivative terms.

Next, we rewrite the Neumann problem (8) in terms of the vector of unknowns

$$\mathbf{u}^{(k+1),n+1} := \left( \mathbf{u}_I^{(2),(k+1),n+1 T} \mathbf{u}_\Gamma^{(k+1),n+1 T} \right)^T.$$

With  $\mathbf{u}^{(k+1),0} = \mathbf{u}(0)$  and  $\mathcal{I}(\underline{\mathbf{q}}^{(k+1)})$ , the implicit Euler scheme for (8) is

$$(\mathbf{M} + \Delta t \mathbf{A}) \mathbf{u}^{(k+1),n+1} = \mathbf{M} \mathbf{u}^{(k+1),n} - \Delta t \begin{pmatrix} \mathbf{0} \\ \mathcal{I}(\underline{\mathbf{q}}^{(k+1)})(t_{n+1}) \end{pmatrix}, \quad n = 0, \dots, N_2^{(k+1)} - 1. \quad (14)$$

Finally, the interfaces values are updated by

$$\mathbf{u}_\Gamma^{(k+1),n} \leftarrow \Theta \mathbf{u}_\Gamma^{(k+1),n} + (1 - \Theta) \mathcal{I}(\underline{\mathbf{u}}_\Gamma^{(k)})(t_n), \quad n = 0, \dots, N_2^{(k+1)}.$$

Algorithm 1 shows a pseudocode of this method.

---

**Algorithm 1** Pseudocode of the DNWR IE method. On domain  $\Omega_m$  we do  $N_m$  timesteps of size  $\Delta t_m = T_f/N_m$ .

---

**DNWR IE**( $T_f, N_1, N_2, (\mathbf{u}_0^{(1)}, \mathbf{u}_0^{(2)}, \mathbf{u}_\Gamma(0)), \Theta, TOL_{WR}, k_{\max}$ ):  
 $\underline{\mathbf{u}}_\Gamma^{(0)} \equiv \mathbf{u}_\Gamma(0)$  Initial guess  
**for**  $k = 0, \dots, k_{\max} - 1$  **do**  
     $\mathcal{I}(\underline{\mathbf{u}}_\Gamma^{(k)}) \leftarrow \text{Interpolation}(\underline{\mathbf{u}}_\Gamma^{(k)})$   
     $\underline{\mathbf{q}}^{(k+1)} \leftarrow \text{SolveDirichlet}(T_f, N_1, \mathbf{u}_0^{(1)}, \mathcal{I}(\underline{\mathbf{u}}_\Gamma^{(k)}))$   
     $\mathcal{I}(\underline{\mathbf{q}}^{(k+1)}) \leftarrow \text{Interpolation}(\underline{\mathbf{q}}^{(k+1)})$   
     $\underline{\mathbf{u}}_\Gamma^{(k+1)} \leftarrow \text{SolveNeumann}(T_f, N_2, (\mathbf{u}_0^{(2)}, \mathbf{u}_0(x_\Gamma)), \mathcal{I}(\underline{\mathbf{q}}^{(k+1)}))$   
     $\underline{\mathbf{u}}_\Gamma^{(k+1)} \leftarrow \Theta \underline{\mathbf{u}}_\Gamma^{(k+1)} + (1 - \Theta) \underline{\mathbf{u}}_\Gamma^{(k)}$   
    **if**  $\|\mathbf{u}_\Gamma^{(k+1), N_2} - \mathbf{u}_\Gamma^{(k), N_2}\|_\Gamma < TOL_{WR} \|\mathbf{u}_\Gamma(0)\|_\Gamma$  **then**  
        **break**  
    **end if**  
**end for**

---

### 5.3 SDIRK2

We now introduce a higher order version of the same multirate algorithm. Specifically, we consider the second order singly diagonally implicit Runge-Kutta (SDIRK2) method as a basis to discretize the systems (5), (8) and (10) in time. For a general IVP  $\dot{\mathbf{u}}(t) = \mathbf{f}(t, \mathbf{u}(t))$ ,  $\mathbf{u}(0) = \mathbf{u}_0$ ,  $t \in [0, T_f]$ , SDIRK2 is defined as follows:

$$\begin{aligned} \mathbf{U}_1 &= \mathbf{u}_n + a\Delta t_n \mathbf{f}(t_n + a\Delta t_n, \mathbf{U}_1), \\ \mathbf{u}_{n+1} = \mathbf{U}_2 &= \mathbf{u}_n + (1 - a)\Delta t_n \mathbf{f}(t_n + a\Delta t_n, \mathbf{U}_1) + a\Delta t_n \mathbf{f}(t_n + \Delta t_n, \mathbf{U}_2), \end{aligned}$$

with  $a = 1 - \frac{1}{2}\sqrt{2}$ . Here, the so-called stage derivatives are

$$\mathbf{k}_1 = \mathbf{f}(t_n + a\Delta t_n, \mathbf{U}_1) \approx \dot{\mathbf{u}}(t_n + a\Delta t_n) \quad \text{and} \quad \mathbf{k}_2 = \mathbf{f}(t_n + \Delta t_n, \mathbf{U}_2) \approx \dot{\mathbf{u}}(t_n + \Delta t_n).$$

In the following we use  $\mathbf{U}_j^{(m)}, \mathbf{k}_j^{(m)}$ ,  $j = 1, 2$ , to denote the stage solutions resp. derivatives on  $\Omega_m$ ,  $m = 1, 2$ .

Using the SDIRK2 scheme to solve the Dirichlet problem (5), with initial value  $\mathbf{u}_I^{(1), (k+1), 0} = \mathbf{u}_I^{(1)}(0)$  and approximating  $\mathbf{U}_1^{(2)}|_\Gamma$  by  $\mathcal{I}(\underline{\mathbf{u}}_\Gamma^{(k)})(t_n + a\Delta t_n)$ , first yields

$$\begin{aligned} & \left( \mathbf{M}_{II}^{(1)} + a\Delta t \mathbf{A}_{II}^{(1)} \right) \mathbf{U}_1^{(1)} \\ &= \mathbf{M}_{II}^{(1)} \mathbf{u}^{(1), (k+1), n} - a\Delta t \left( \mathbf{M}_{II}^{(1)} \frac{d}{dt} \mathcal{I}(\underline{\mathbf{u}}_\Gamma^{(k)})(t_n + a\Delta t_n) + \mathbf{A}_{II}^{(1)} \mathcal{I}(\underline{\mathbf{u}}_\Gamma^{(k)})(t_n + a\Delta t_n) \right). \end{aligned} \quad (15)$$

We then compute the stage heat flux

$$\mathbf{q}_1^{(k+1), n+1} = \mathbf{M}_{\Gamma I}^{(1)} \mathbf{k}_1^{(1)} + \mathbf{A}_{\Gamma I}^{(1)} \mathbf{U}_1^{(1)} + \mathbf{M}_{\Gamma \Gamma}^{(1)} \frac{d}{dt} \mathcal{I}(\underline{\mathbf{u}}_\Gamma^{(k)})(t_n + a\Delta t_n) + \mathbf{A}_{\Gamma I}^{(1)} \mathcal{I}(\underline{\mathbf{u}}_\Gamma^{(k)})(t_n + a\Delta t_n). \quad (16)$$

In both (15) and (16), we approximate the derivative terms by

$$\frac{d}{dt} \mathcal{I}(\underline{\mathbf{u}}_\Gamma^{(k)})(t_n + a\Delta t_n) \approx \left( \mathcal{I}(\underline{\mathbf{u}}_\Gamma^{(k)})(t_n + a\Delta t_n) - \mathcal{I}(\underline{\mathbf{u}}_\Gamma^{(k)})(t_n) \right) / (a\Delta t_n).$$

For the second SDIRK2 stage, one solves

$$\begin{aligned} & \left( \mathbf{M}_{II}^{(1)} + a\Delta t \mathbf{A}_{II}^{(1)} \right) \mathbf{u}_I^{(1),(k+1),n+1} \\ &= \mathbf{M}_{II}^{(1)} \left( \mathbf{u}^{(1),(k+1),n} + (1-a)\Delta t_n \mathbf{k}_1^{(1)} \right) \\ & \quad - a\Delta t \left( \mathbf{M}_{II}^{(1)} \frac{d}{dt} \mathcal{I}(\mathbf{u}_\Gamma^{(k)})(t_n + \Delta t_n) + \mathbf{A}_{II}^{(1)} \mathcal{I}(\mathbf{u}_\Gamma^{(k)})(t_n + \Delta t) \right), \end{aligned}$$

and computes the second heat flux

$$\begin{aligned} \mathbf{q}_2^{(k+1),n+1} &= \mathbf{M}_{II}^{(1)} \mathbf{k}_2^{(1)} + \mathbf{A}_{II}^{(1)} \mathbf{u}_I^{(1),(k+1),n+1} \\ & \quad + \mathbf{M}_{II}^{(1)} \frac{d}{dt} \mathcal{I}(\mathbf{u}_\Gamma^{(k)})(t_n + \Delta t_n) + \mathbf{A}_{II}^{(1)} \mathcal{I}(\mathbf{u}_\Gamma^{(k)})(t_n + \Delta t_n). \end{aligned}$$

In the computation of the second stage, we use the derivative approximation

$$\begin{aligned} & \frac{d}{dt} \mathcal{I}(\mathbf{u}_\Gamma^{(k)})(t_n + \Delta t_n) \\ & \approx \left( \mathcal{I}(\mathbf{u}_\Gamma^{(k)})(t_n + \Delta t_n) - \left( \mathcal{I}(\mathbf{u}_\Gamma^{(k)})(t_n) + (1-a)\Delta t_n \frac{d}{dt} \mathcal{I}(\mathbf{u}_\Gamma^{(k)})(t_n + a\Delta t_n) \right) \right) / (a\Delta t_n). \end{aligned}$$

This procedure is repeated for all  $n = 0, \dots, N_1^{(k+1)} - 1$ . The time-point evaluations in our derivative approximations coincide with the time-points for which the SDIRK2 scheme provides discrete solutions, in case of matching time-grids on both subdomains.

We now construct the two interpolants  $\mathcal{I}(\mathbf{q}_1^{(k+1)})$  and  $\mathcal{I}(\mathbf{q}_2^{(k+1)})$ , where the former corresponds to the time-points  $0, a\Delta t_0, t_1 + a\Delta t_1, \dots$ . We compute the initial flux  $\mathbf{q}^{(k+1),0}$ , which we use in both flux interpolants, using the second order forward differences:

$$\begin{aligned} \frac{d}{dt} \mathcal{I}(\mathbf{u}_\Gamma^{(k)})(0) &\approx \frac{-(1-c^2)\mathcal{I}(\mathbf{u}_\Gamma^{(k)})(0) + \mathcal{I}(\mathbf{u}_\Gamma^{(k)})(\Delta t_0) - c^2\mathcal{I}(\mathbf{u}_\Gamma^{(k)})(\Delta t_0 + \Delta t_1)}{\Delta t_0(1-c)}, \\ \dot{\mathbf{u}}_I^{(1),(k)}(0) &\approx \frac{-(1-c^2)\mathbf{u}_I^{(1),(k),0} + \mathbf{u}_I^{(1),(k),1} - c^2\mathbf{u}_I^{(1),(k),2}}{\Delta t_0(1-c)}, \\ c &= \frac{\Delta t_0}{\Delta t_0 + \Delta t_1}. \end{aligned}$$

Using the SDIRK2 scheme to solve the Neumann problem (8), replacing the heat flux by  $\mathcal{I}(\mathbf{q}_1^{(k+1)})$  resp.  $\mathcal{I}(\mathbf{q}_2^{(k+1)})$ , consists of first solving

$$(\mathbf{M} + a\Delta t \mathbf{A}) \mathbf{U}_1^{(2)} = \mathbf{M} \mathbf{u}^{(k+1),n} - a\Delta t_n \begin{pmatrix} \mathbf{0} \\ \mathcal{I}(\mathbf{q}_1^{(k+1)})(t_n + a\Delta t_n) \end{pmatrix},$$

followed by

$$(\mathbf{M} + a\Delta t \mathbf{A}) \mathbf{u}^{(2),(k+1),n+1} = \mathbf{M} \left( \mathbf{u}^{(k+1),n} + (1-a)\Delta t_n \mathbf{k}_1^{(2)} \right) - a\Delta t \begin{pmatrix} \mathbf{0} \\ \mathcal{I}(\mathbf{q}_2^{(k+1)})(t_n + \Delta t_n) \end{pmatrix},$$

for  $n = 0, \dots, N_2^{(k+1)} - 1$ . The relaxation step and termination check are identical to the implicit Euler method. Here, we use a total of only 3 interpolants: The solution, the heat flux and the stage heat flux. This was achieved by the approximation of  $\mathbf{U}_1^{(2)}|_\Gamma$  by  $\mathcal{I}(\mathbf{u}_\Gamma^{(k)})$ . As can be seen in the numerical results in Section 8.3, this does not lead to a loss of order. Other options for constructing partitioned time-integration methods based on SDIRK2 are discussed in [28, Chap. 5].

The differences to Algorithm 1 are in `SolveDirichlet` and `SolveNeumann`, which require solving two linear systems each. Additionally, `SolveDirichlet` now returns two heat fluxes, which are both interpolated and passed into `SolveNeumann`.



## 5.4 Optimal relaxation parameter

By writing out the linear system for all timesteps in a single WR iteration, one can see that the iteration matrix is a block lower-triangular Toeplitz matrix. Thus, its spectral radius is independent of the number of timesteps, c.f., [20]. This means it is sufficient to look at a single timestep to determine the optimal relaxation parameter. In this setting the iteration matrix w.r.t.  $\mathbf{u}_\Gamma^{(k)}$  was already determined in [30]. It is given by

$$\mathbf{\Sigma} = -\mathbf{S}^{(2)-1}\mathbf{S}^{(1)},$$

where

$$\mathbf{S}^{(m)} := \left( \frac{\mathbf{M}_{\Gamma\Gamma}^{(m)}}{\Delta t} + \mathbf{A}_{\Gamma\Gamma}^{(m)} \right) - \left( \frac{\mathbf{M}_{\Gamma I}^{(m)}}{\Delta t} + \mathbf{A}_{\Gamma I}^{(m)} \right) \left( \frac{\mathbf{M}_{II}^{(m)}}{\Delta t} + \mathbf{A}_{II}^{(m)} \right)^{-1} \left( \frac{\mathbf{M}_{I\Gamma}^{(m)}}{\Delta t} + \mathbf{A}_{I\Gamma}^{(m)} \right). \quad (17)$$

This is obtained by solving (12) for  $\mathbf{u}_I^{(1),(k+1),n+1}$ , assuming  $\mathbf{u}_I^{(1),(k+1),n} = \mathbf{0}$ . Insert this result into (13) and then (14). Lastly, solve (14) for  $\mathbf{u}_\Gamma^{(k+1),n+1}$ , assuming  $\mathbf{u}_I^{(2),(k+1),n} = \mathbf{0}$ , using the Schur-complement.

Including the relaxation step yields the following iteration (for a single timestep):

$$\mathbf{u}_\Gamma^{(k+1)} = (\Theta \mathbf{\Sigma} + (1 - \Theta) \mathbf{I}) \mathbf{u}_\Gamma^{(k)}.$$

In the 1D case  $\mathbf{S}^{(m)}$  and  $\mathbf{\Sigma}$  are scalars, thus the optimal relaxation parameter is

$$\Theta_{opt} = \frac{1}{\left| 1 + \mathbf{S}^{(2)-1}\mathbf{S}^{(1)} \right|}. \quad (18)$$

In the following we specifically consider a 1D model problem on  $\Omega = [-1, 1]$ , split at  $x_\Gamma = 0$ , and an equidistant discretization using linear finite elements. The matrices  $\mathbf{M}_{II}^{(m)}$  and  $\mathbf{A}_{II}^{(m)}$  have a known Toeplitz structure. Thus, one can write down an exact expression of (17) using an Eigendecomposition to calculate the inverse of  $\mathbf{M}_{II}^{(m)}/\Delta t + \mathbf{A}_{II}^{(m)}$ . Through lengthy but straight forward calculations (see [30, 29]), one obtains the following expressions:

$$\begin{aligned} \mathbf{S}^{(m)} &= \frac{6\Delta t \Delta x (\alpha_m \Delta x^2 + 3\lambda_m \Delta t) - (\alpha_m \Delta x^2 - 6\lambda_m \Delta t)^2 s_m}{18\Delta t \Delta x^3}, \\ s_m &= \sum_{i=1}^N \frac{3\Delta t \Delta x^2 \sin^2(i\pi \Delta x)}{2\alpha_m \Delta x^2 + 6\lambda_m \Delta t + (\alpha_m \Delta x^2 - 6\lambda_m \Delta t) \cos(i\pi \Delta x)}. \end{aligned} \quad (19)$$

Using  $c = \Delta t / \Delta x^2$ ,  $\Theta_{opt}$  has the following temporal and spatial limits [30]:

$$\lim_{c \rightarrow 0} \Theta_{opt} = \frac{\alpha_2}{\alpha_1 + \alpha_2}, \quad \lim_{c \rightarrow \infty} \Theta_{opt} = \frac{\lambda_2}{\lambda_1 + \lambda_2}. \quad (20)$$

These are consistent with the one-dimensional continuous analysis performed in [13, 25]. There, a convergence analysis using Laplace transforms for the DNWR method (2)-(4) on two identical subdomains  $\Omega_1$  and  $\Omega_2$  with constant coefficients shows that  $\Theta_{opt} = 1/2$ . Their result is recovered when approaching the continuous case in the limit  $\Delta t / \Delta x^2 \rightarrow \infty$  for constant coefficients.

Figure 2 shows  $\Theta_{opt}$  for a few material combinations, see Table 1. One can observe that  $\Theta_{opt}$  is continuous and bounded by its spatial and temporal limits (20).

### 5.4.1 Multirate relaxation parameter

For  $\Delta t_1 \neq \Delta t_2$  the analysis in the previous section does not apply anymore. Instead, we determine  $\Theta_{opt}$  based on numerical experiments in Section 8.1. These show that, on average, the optimal choice is to use  $\Theta_{opt}$  based on the maximum of  $\Delta t_1$  and  $\Delta t_2$ . This result coincides with the experiments to determine  $\Theta_{opt}$  for the multirate NNWR method in [33].

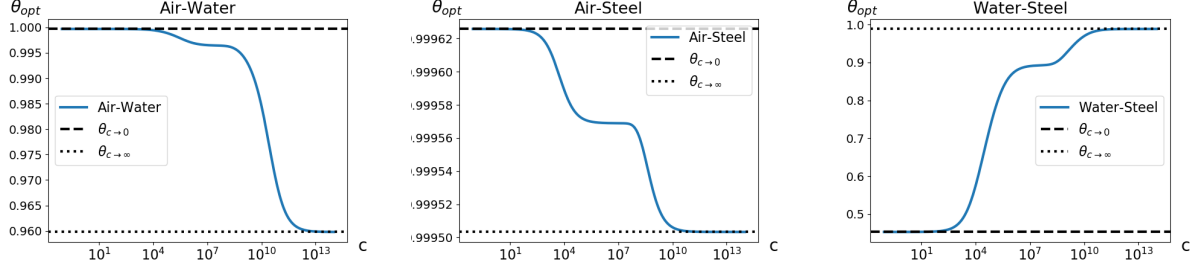


Figure 2:  $\Theta_{opt}$  over  $\Delta t/\Delta x^2$  for DNWR algorithm.  $\Delta x = 1/100$ ,  $T_f = 10^{10}$  and  $\Delta t = T_f/2^0, \dots, T_f/2^{50}$ .

## 6 Time adaptive method

The goal of adaptivity is to use step-sizes as large as possible and as small as necessary to reduce computational costs, while ensuring a target accuracy. In particular, using adaptive time stepping for both sub-domains separately, one can attain comparable time-integration errors automatically, bypassing the need to determine a suitable step-size ratio for the multirate case.

The basic idea is to control timestepsizes to keep an error estimate at a given tolerance  $TOL$ . We use a local error estimate obtained by an embedded technique [17, chap. IV.8]. With the SDIRK2 method, we obtain a lower order embedded solution  $\hat{\mathbf{u}}_{n+1}$  via

$$\hat{\mathbf{u}}_{n+1} = \mathbf{u}_n + (1 - \hat{a})\Delta t_n \mathbf{k}_1 + \hat{a}\Delta t_n \mathbf{k}_2, \quad \hat{a} = 2 - \frac{5}{4}\sqrt{2}.$$

The local error estimate is  $\ell_n = \mathbf{u}_n - \hat{\mathbf{u}}_n$ . We then control timesteps using the proportional-integral (PI) controller

$$\Delta t_{n+1} = \Delta t_n \left( \frac{TOL}{\|\ell_n\|_I} \right)^{1/3} \left( \frac{TOL}{\|\ell_{n-1}\|_I} \right)^{-1/6},$$

cf. [1], PI3333. We use this procedure on each subdomain independently. As the initial stepsize we use

$$\Delta t_0^{(m)} = \frac{T_f TOL^{(m)1/2}}{100(1 + \|\mathbf{M}_{II}^{(m)-1} \mathbf{A}_{II}^{(m)} \mathbf{u}_I^{(m)}(0)\|_I)}, \quad m = 1, 2,$$

c.f. [33]. We choose the tolerances  $TOL^{(m)} = TOL_{WR}/5$ ,  $m = 1, 2$ . This choice is motivated by [36] and already used in a similar context in [4, 33]. We use the discrete  $\mathcal{L}^2$  norm

$$\|\mathbf{u}\|_I^2 = (\mathbf{u}^T \mathbf{M} \mathbf{u})/|\Omega_u|, \quad (21)$$

where  $\mathbf{M}$  is the corresponding mass matrix and  $|\Omega_u|$  the area on which  $\mathbf{u}$  is defined.

Using this adaptive method, we get independent time-grids for both sub-domains, that are suitable for the given material parameters. A pseudocode of the adaptive SDIRK2 DNWR method is shown in Algorithm 2.

### 6.1 Relaxation parameter

In the adaptive method the Dirichlet-Neumann operator changes every WR step, since the timestepsizes change. Consequently, we recompute  $\Theta$  in every iteration. We use  $\Theta$  as in the multirate case with the average stepsizes from each subdomain. This approach improves upon [33], where  $\Theta$  was based on the timegrids of the previous WR iteration.

---

**Algorithm 2** Pseudocode of the adaptive SDIRK2 DNWR method. The functions `AdaptiveSolveDirichlet` and `AdaptiveSolveNeumann` perform the time integration from Section 5.3, using the step-size control from Section 6. Note that the time-grids associated with  $\underline{\mathbf{u}}_\Gamma^{(k)}$ ,  $\underline{\mathbf{q}}_1^{(k+1)}$  and  $\underline{\mathbf{q}}_2^{(k+1)}$  can change in every iteration. This is particularly relevant in the relaxation step, where one needs to interpolate the previous solution to the new time-grid.

---

```

DNWR_SDIRK2_TA( $T_f, (\mathbf{u}_0^{(1)}, \mathbf{u}_0^{(2)}, \mathbf{u}_\Gamma(0)), \Theta, TOL_{WR}, k_{\max}$ ):
 $\mathbf{u}_\Gamma^{(0)} \equiv \mathbf{u}_\Gamma(0)$  Initial guess
for  $k = 0, \dots, k_{\max} - 1$  do
     $\mathcal{I}(\mathbf{u}_\Gamma^{(k)}) \leftarrow \text{Interpolation}(\mathbf{u}_\Gamma^{(k)})$ 
     $\underline{\mathbf{q}}_1^{(k+1)}, \underline{\mathbf{q}}_2^{(k+1)} \leftarrow \text{AdaptiveSolveDirichlet}(T_f, TOL/5, \mathbf{u}_0^{(1)}, \mathcal{I}(\mathbf{u}_\Gamma^{(k)}))$ 
     $\mathcal{I}(\underline{\mathbf{q}}_1^{(k+1)}) \leftarrow \text{Interpolation}(\underline{\mathbf{q}}_1^{(k+1)})$ 
     $\mathcal{I}(\underline{\mathbf{q}}_2^{(k+1)}) \leftarrow \text{Interpolation}(\underline{\mathbf{q}}_2^{(k+1)})$ 
     $\mathbf{u}_\Gamma^{(k+1)} \leftarrow \text{AdaptiveSolveNeumann}(T_f, TOL/5, (\mathbf{u}_0^{(2)}, \mathbf{u}_0(x_\Gamma)), \mathcal{I}(\underline{\mathbf{q}}_1^{(k+1)}), \mathcal{I}(\underline{\mathbf{q}}_2^{(k+1)}))$ 
    Compute  $\Theta^{(k)}$ , see Section 6.1
     $\mathbf{u}_\Gamma^{(k+1)} \leftarrow \Theta^{(k)} \mathbf{u}_\Gamma^{(k+1)} + (1 - \Theta^{(k)}) \mathbf{u}_\Gamma^{(k)}$ 
    if  $\|\mathbf{u}_\Gamma^{(k+1)}(T_f) - \mathbf{u}_\Gamma^{(k)}(T_f)\|_\Gamma < TOL_{WR} \|\mathbf{u}_\Gamma(0)\|_\Gamma$  then
        break
    end if
end for

```

---

## 7 The Neumann-Neumann Waveform Relaxation algorithm

Here, we briefly recap the related Neumann-Neumann Waveform relaxation (NNWR) method, c.f. [23, 31, 33]. Similar to DNWR, NNWR solves (1) in a partitioned manner. The continuous formulation of the algorithm is as follows: Given  $g^{(k)}(\mathbf{x}, t)$  one first solves the following Dirichlet problem on each subdomain:

$$\begin{aligned}
 \alpha_m \frac{\partial u_m^{(k+1)}(\mathbf{x}, t)}{\partial t} - \nabla \cdot (\lambda_m \nabla u_m^{(k+1)}(\mathbf{x}, t)) &= 0, \quad (\mathbf{x}, t) \in \Omega_m \times (0, T_f], \\
 u_m^{(k+1)}(\mathbf{x}, t) &= 0, \quad (\mathbf{x}, t) \in \partial\Omega_m \setminus \Gamma \times [0, T_f], \\
 u_m^{(k+1)}(\mathbf{x}, t) &= g^{(k)}(\mathbf{x}, t), \quad (\mathbf{x}, t) \in \Gamma \times (0, T_f], \\
 u_m^{(k+1)}(\mathbf{x}, 0) &= u_m^0(\mathbf{x}), \quad \mathbf{x} \in \Omega_m.
 \end{aligned}$$

Next, one solves the following Neumann problems:

$$\begin{aligned}
 \alpha_m \frac{\partial \psi_m^{(k+1)}(\mathbf{x}, t)}{\partial t} - \nabla \cdot (\lambda_m \nabla \psi_m^{(k+1)}(\mathbf{x}, t)) &= 0, \quad (\mathbf{x}, t) \in \Omega_m \times (0, T_f], \\
 \psi_m^{(k+1)}(\mathbf{x}, t) &= 0, \quad (\mathbf{x}, t) \in \partial\Omega_m \setminus \Gamma \times [0, T_f], \\
 \lambda_m \frac{\partial \psi_m^{(k+1)}(\mathbf{x}, t)}{\partial \mathbf{n}_m} &= \lambda_1 \frac{\partial u_1^{(k+1)}(\mathbf{x}, t)}{\partial \mathbf{n}_1} + \lambda_2 \frac{\partial u_2^{(k+1)}(\mathbf{x}, t)}{\partial \mathbf{n}_2}, \quad (\mathbf{x}, t) \in \Gamma \times (0, T_f], \\
 \psi_m^{(k+1)}(\mathbf{x}, 0) &= 0, \quad \mathbf{x} \in \Omega_m.
 \end{aligned} \tag{22}$$

Finally, the update step is

$$g^{(k+1)}(\mathbf{x}, t) = g^{(k)}(\mathbf{x}, t) - \Theta(\psi_1^{(k+1)}(\mathbf{x}, t) + \psi_2^{(k+1)}(\mathbf{x}, t)), \quad (\mathbf{x}, t) \in \Gamma \times [0, T_f].$$

For the fully discrete version and a detailed algorithmic description see [31].

One can solve on the subdomains in parallel. The NNWR algorithm is based on the exact same Dirichlet and Neumann problems as the DNWR algorithm, but with different input data, namely fluxes and initial value for the Neumann problem (22). Hence one can directly use the time-discretizations as described in Section 5, including time-adaptivity, c.f. [33].

Under the same restrictions as in Section 5.4, i.e.,  $\Omega = [-1, 1]$ , split at  $x_\Gamma = 0$  and linear finite elements on an equidistant grid, one can analogously calculate  $\Theta_{opt}$ :

$$\Theta_{opt} = \frac{1}{|2 + \mathbf{S}^{(1)-1} \mathbf{S}^{(2)} + \mathbf{S}^{(2)-1} \mathbf{S}^{(1)}|} \quad (23)$$

with  $\mathbf{S}^{(m)}$  given by (19), see [31] for details. The spatial and temporal limits based on  $c = \Delta t / \Delta x^2$  are

$$\lim_{c \rightarrow 0} \Theta_{opt} = \frac{\alpha_1 \alpha_2}{(\alpha_1 + \alpha_2)^2}, \quad \lim_{c \rightarrow \infty} \Theta_{opt} = \frac{\lambda_1 \lambda_2}{(\lambda_1 + \lambda_2)^2}. \quad (24)$$

## 8 Numerical results

We now present numerical experiments to illustrate the validity of the theoretical results and to test the robustness of the relaxation parameters in 2D, SDIRK2 and with multirate resp. adaptive time-grids. The methods and algorithms described have been implemented in Python 3.6, the code is available at [34].

We consider the domains  $\Omega = [-1, 1]$  for 1D and  $\Omega = [-1, 1] \times [0, 1]$  for 2D, with  $\Omega_1$  and  $\Omega_2$  split at  $x_\Gamma = 0$ . Our initial conditions are

$$u(x) = 500 \sin((x+1)\pi/2), \quad \text{resp.} \quad u(x, y) = 500 \sin((x+1)\pi/2) \sin(y\pi). \quad (25)$$

As the coefficients  $\alpha$  and  $\lambda$  in (1) we consider the materials as shown in Table 1.

Material	$\alpha = \rho \cdot c_p [J/(K m^3)]$	$\lambda [W/(mK)]$
Air	$1.293 \cdot 1005$	0.0243
Water	$999.7 \cdot 4192.1$	0.58
Steel	$7836 \cdot 443$	48.9

Table 1: Material parameters.

The resulting heterogeneous cases are Air-Water, Air-Steel and Water-Steel. We use  $T_f = 10^4$  in all cases.

As space discretization we use linear finite elements on equidistant grids (1D:  $\Delta x = 1/200$ , 2D:  $\Delta x = 1/100$ ) as shown in Figure 1, see [4] for more details. The resulting linear equation systems are solved with direct solvers.

We define our multirate setup via  $N$  as the number of base timesteps. In subdomain  $\Omega_m$  we then use  $N_m = c_m \cdot N$  timesteps. We consider the following cases: Coarse-coarse ( $c_1 = c_2 = 1$ ), coarse-fine ( $c_1 = 1, c_2 = 10$ ) and fine-coarse ( $c_1 = 10, c_2 = 1$ ).

### 8.1 Multirate relaxation parameter

The question is what  $\Theta$  to choose for DNWR in the multirate case, i.e., which  $\Delta t$  to use in (19). We consider the following four choices: **Max/Min/Avg** by taking the maximum, minimum or average of  $\Delta t_1$  and  $\Delta t_2$  to compute  $\Theta_{opt}$ , and **Mix**:  $\Theta_{opt} = 1/(|1 + \mathbf{S}^{(2)-1}(\Delta t_2) \mathbf{S}^{(1)}(\Delta t_1)|)$ .

We experimentally determine the convergence rate via

$$\|\mathbf{u}_\Gamma^{(k)}(T_f) - \mathbf{u}_\Gamma^{(k-1)}(T_f)\|_\Gamma / \|\mathbf{u}_\Gamma^{(k-1)}(T_f) - \mathbf{u}_\Gamma^{(k-2)}(T_f)\|_\Gamma, \quad (26)$$

i.e., the reduction rate in the update. Here, we perform up to  $k_{\max} = 6$  iterations and take the mean of the update reductions, but never the last iteration, which could be near machine

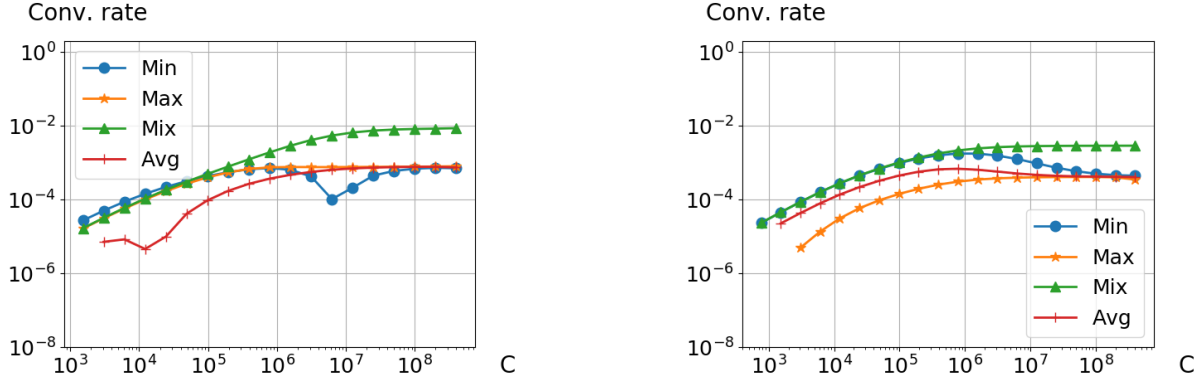


Figure 3: Observed convergence rates over  $c = \Delta t/\Delta x^2$  for DNWR IE, 1D, air-water. Left: Coarse-fine. Right: Fine-coarse.

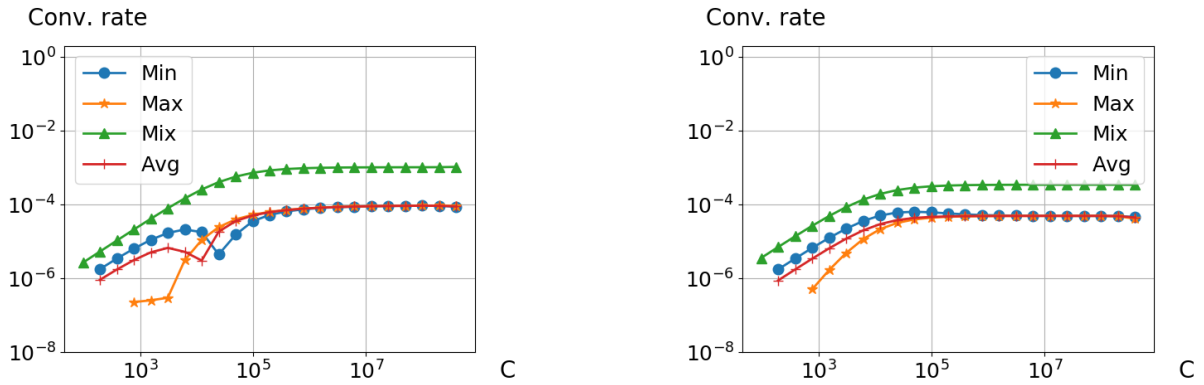


Figure 4: Observed convergence rates over  $c = \Delta t/\Delta x^2$  for DNWR IE, 1D, air-steel. Left: Coarse-fine. Right: Fine-coarse.

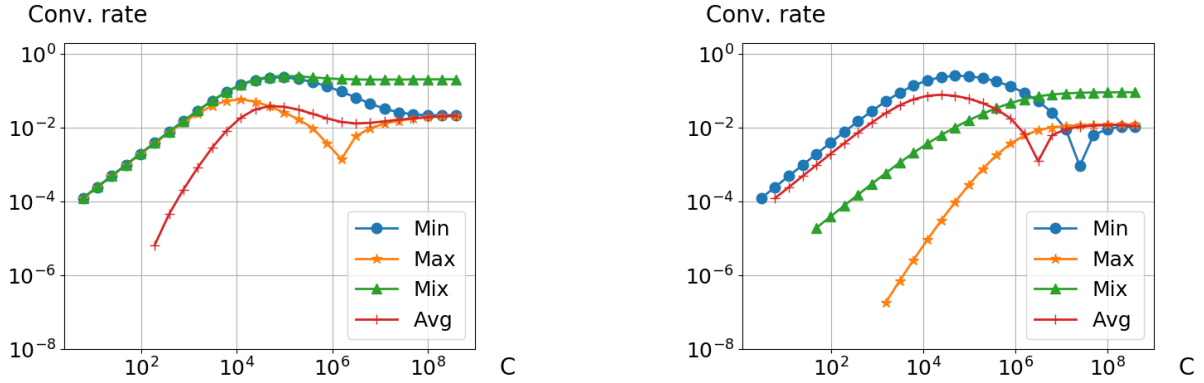


Figure 5: Observed convergence rates over  $c = \Delta t/\Delta x^2$  for DNWR IE, 1D, water-steel. Left: Coarse-fine. Right: Fine-coarse.

precision. This experiment is done using IE for the 1D test case and  $N = 1$ , as we aim to determine the asymptotic convergence rates.

The results in Figures 3, 4 and 5 show that all options yield comparable results, with "Max" being most consistent, making it our choice for DNWR in the multirate setting.

Numerical experiments in [31] yielded the same conclusion for the NNWR method. As such we use (23) based on the larger step-size.

## 8.2 Optimality of relaxation parameter

We now verify the optimality of the relaxation parameters (18) for DNWR and (23) for NNWR in 1D with implicit Euler and also test the convergence rate and robustness. To this end, we determine the experimental convergences rates as in Section 8.1, for varying  $\Theta$  in 1D and 2D for both implicit Euler and SDIRK2. Time-integration is done in multirate and non-multirate, up to  $T_f$  using  $N = 100$  base timesteps.

We expect little variation for implicit Euler and SDIRK2, since SDIRK2 consists of two successive implicit Euler steps. We anticipate more notable differences between 1D and 2D. Lastly, convergence rates might deviate due to transitive effects of WR, since the iteration matrices are non-normal.

In the plots, the blue highlighted range on the  $x$ -axis marks the spatial and temporal limits of  $\Theta$ , see (20) resp. (24).

### 8.2.1 DNWR

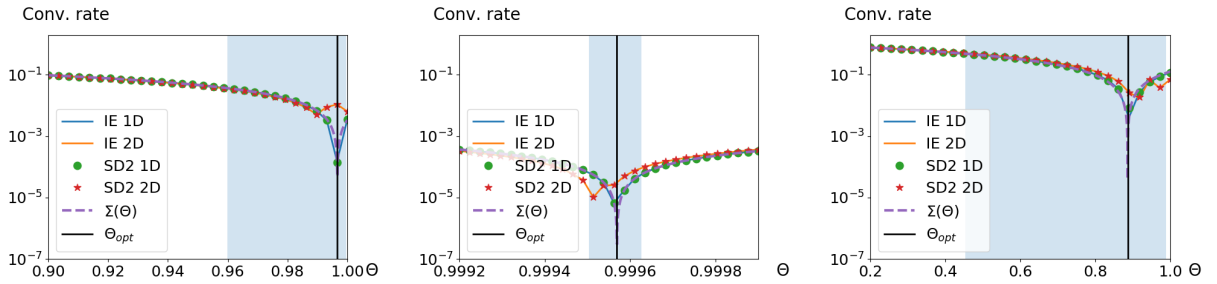


Figure 6: Left: Air-water, fine-coarse. Centre: Air-steel, coarse-coarse. Right: Water-steel, coarse-fine. Observed convergence rates for DNWR algorithm.

Results are seen in Figure 6. In both 1D and 2D, SDIRK2 rates match those of implicit Euler. In all cases, 1D results closely align with the theoretical result marked by  $\Sigma(\Theta)$ . 2D results are slightly off, but still yield good error reduction rates using the 1D  $\Theta_{opt}$ . For air-water, the error reduction rate is  $\approx 10^{-2}$ , i.e., the coupling residual gains two decimals in accuracy per iteration. The air-steel coupling yields very fast convergence with an error reduction rate of  $\approx 10^{-4}$  and water-steel rates are between 0.1 and 0.01 for  $\Theta_{opt}$ .

Additionally, we see that DNWR is convergent for all shown  $\Theta$ . Thus, in the worst case DNWR convergence is slow, yet not divergent.

### 8.2.2 DNWR - non-square geometry

We test if the DNWR results extend to non-square domains. In particular, we consider the spatial domain with  $x \in [-9, 1]$ ,  $x_\Gamma = 0$ . We use the initial conditions

$$u(x) = 500 \sin((x + 9)\pi/10), \quad \text{resp.} \quad u(x, y) = 500 \sin((x + 9)\pi/10) \sin(y\pi).$$

We test only the non-multirate setting. Results are shown in Figure 7 and strongly resemble the results for square, identical domains in Figure 6, except for slower convergence rates for the 2D water-steel case.

This similarity can be explained by looking at the Schur-complements (17).  $\mathbf{M}_{\Gamma\Gamma}^{(m)}$  and  $\mathbf{A}_{\Gamma\Gamma}^{(m)}$  remain unchanged.  $\mathbf{M}_{II}^{(1)}$  resp.  $\mathbf{A}_{II}^{(1)}$  increase in size, but values and structure persist. The matrices  $\mathbf{M}_{\Gamma I}^{(1)}$ ,  $\mathbf{A}_{\Gamma I}^{(1)}$  and  $\mathbf{M}_{I\Gamma}^{(1)}$ ,  $\mathbf{A}_{I\Gamma}^{(1)}$  are padded with additional zeros. The increased size of  $\mathbf{M}_{II}^{(1)}/\Delta t + \mathbf{A}_{II}^{(1)}$  does affect its inverse, but after multiplication with  $\mathbf{M}_{\Gamma I}^{(1)}/\Delta t + \mathbf{A}_{\Gamma I}^{(1)}$  and  $\mathbf{M}_{I\Gamma}^{(1)}/\Delta t + \mathbf{A}_{I\Gamma}^{(1)}$ , which are mostly zero, the effect on  $\mathbf{S}^{(1)}$  is expected to be minor.

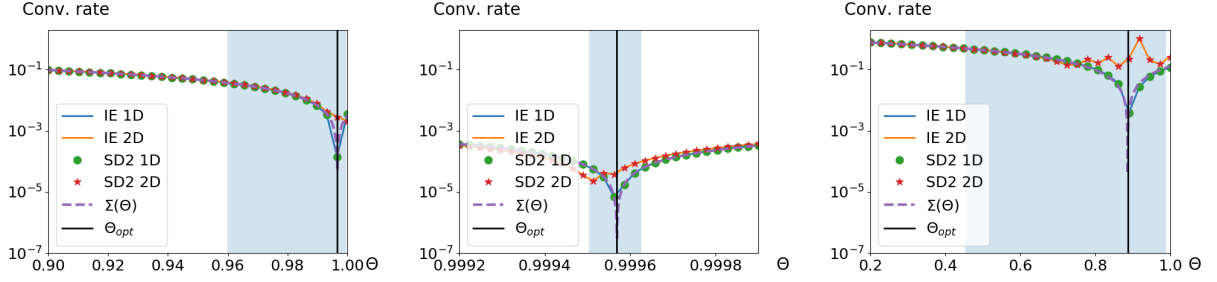


Figure 7: Left: Air-water. Centre: Air-steel. Right: Water-steel. Observed convergence rates for DNWR algorithm using non-square geometry and matching step-sizes.

### 8.2.3 NNWR

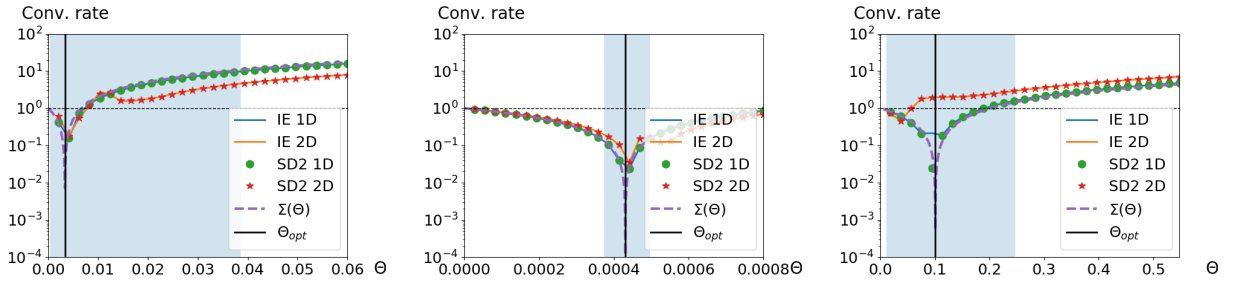


Figure 8: Left: Air-water, fine-coarse. Centre: Air-steel, coarse-coarse. Right: Water-steel, coarse-fine. Observed convergence rates for NNWR algorithm.

Results are shown in Figure 8. We additionally mark the divergence limit at 1, showing the range of viable  $\Theta$  is very small for NNWR and unlike DNWR, relaxation is non-optional for convergence. In particular, one may get divergence for  $\Theta$  within the range marked by the temporal and spatial limits. Convergence rates for implicit Euler and SDIRK2 results are almost identical. 1D convergence rates align well with the theoretical results in all cases. In 2D, the air-water and air-steel results match with the 1D results, yielding rates of about 0.01–0.1. However, water-steel shows divergence in 2D, when using  $\Theta_{opt}$ . In the convergent cases, the observed error reduction rates are slower than for DNWR, this is particularly pronounced in the air-steel case, with a difference of about 3 orders of magnitude. Overall, NNWR shows a lack of robustness.

One might achieve better convergence rates using macrostepping, i.e., successively performing the algorithm on smaller time-windows. This may speed up convergence on each time-window, but the coupling residual propagates through erroneous initial values. On the other hand, DNWR performs well on the given time-windows.

### 8.3 Multirate - convergence order of time-integration

We show convergence of the error, on the whole domain in the discrete  $\mathcal{L}^2$  norm (21) and using  $T_f = 1$ , for  $\Delta t \rightarrow 0$ . Our reference solution is the monolithic solution for sufficiently small step-sizes, thus measuring both the time-integration error and coupling residual.

Results for  $TOL_{WR} = 10^{-13}$  can be seen in Figure 9 for DNWR and in Figure 10 for NNWR. We attain the expected first and second order convergence rates for  $\Delta t \rightarrow 0$ .

### 8.4 Time adaptive results

We consider the time-adaptive DNWR method described in Section 6. The reference for error computation is the solution using  $TOL_{WR} = 10^{-8}$  in 1D and  $TOL_{WR} = 10^{-7}$  in 2D. We expect

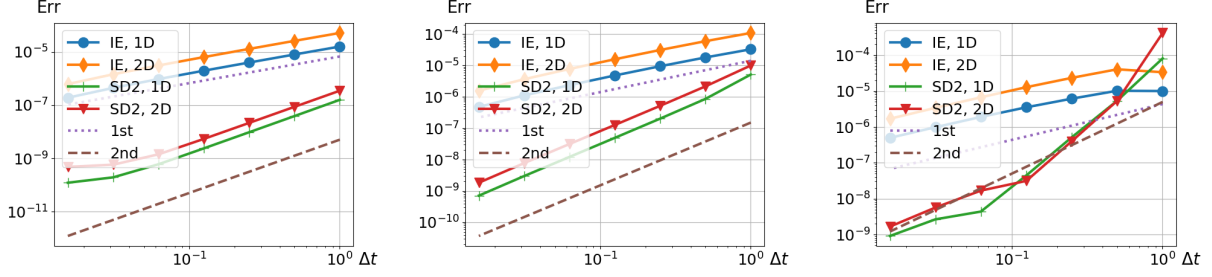


Figure 9: Left: Air-water, fine-coarse. Centre: Air-steel, coarse-coarse. Right: Water-steel, coarse-fine. Error over  $\Delta t$  for DNWR and  $T_f = 1$ .

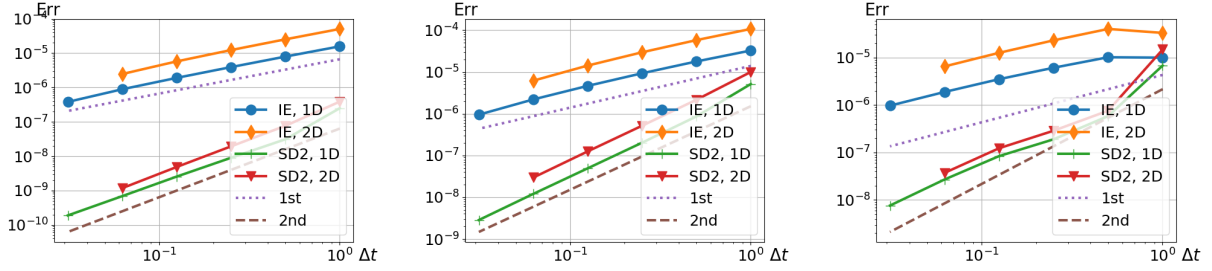


Figure 10: Left: Air-water, fine-coarse. Centre: Air-steel, coarse-coarse. Right: Water-steel, coarse-fine. Error over  $\Delta t$  for NNWR and  $T_f = 1$ .

the errors to be proportional to the tolerance for  $TOL_{WR} \rightarrow 0$ , which is observed in Figure 11. Due to its lacking robustness, we do not consider time-adaptive NNWR.

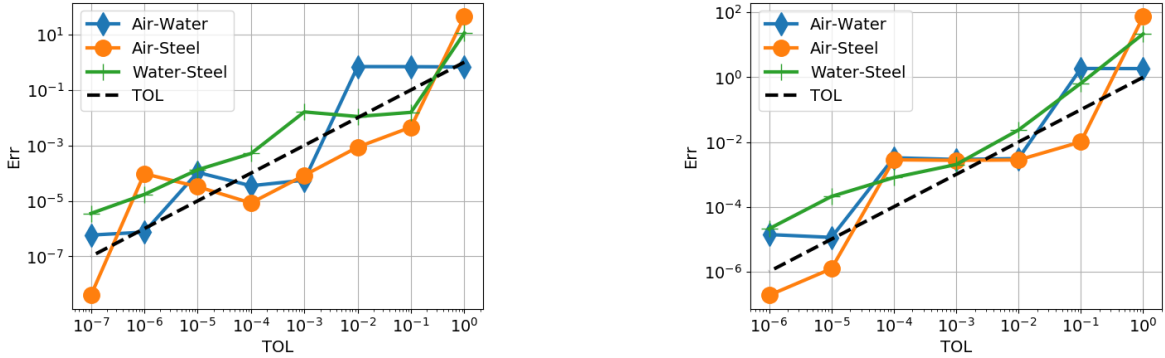


Figure 11: Left: 1D. Right: 2D. Error over  $TOL_{WR}$  for the time-adaptive DNWR method.

#### 8.4.1 Error over work comparison

We now compare efficiency of the adaptive and multirate method for the 2D test case with  $\Delta x = 1/200$ . For this we compare error over work, which we measure as the total number of timesteps.

We choose the stepsize ratios in the multirate setting such that both domains use comparable  $CFL$  numbers, which is achieved by  $c_2 = c_1 D_2/D_1$ ,  $D_m = \lambda_m/\alpha_m$ ,  $m = 1, 2$ . However, we require  $c_m \in \mathbb{N}$ . W.l.o.g., assume  $D_2/D_1 > 1$ , we then set  $c_1 = 1$  and round down  $c_2 = D_2/D_1$ . See Table 2 for the resulting stepsize ratios for our material configurations.



To compare the multirate method with the time-adaptive method, we parametrize the former by the number of base timesteps  $N$ . Given  $\Delta t_m = T_f/(c_m \cdot N)$ ,  $m = 1, 2$ , we compute the associated time integration error  $e_{\Delta t_1, \Delta t_2}$  using  $TOL_{WR} = 10^{-12}$  and a monolithic reference solution with  $\Delta t = \min(\Delta t_1, \Delta t_2)/2$ . We then use  $TOL_{WR} = e_{\Delta t_1, \Delta t_2}/5$  in the termination criterion for the multirate method, for its error over work comparison. Finally, our references for the error computations in the error over work comparison are adaptive solutions with  $TOL_{WR} = 10^{-6}$ .

Results are shown in Figure 12 with the resulting stepsizes ratios for the adaptive case in Table 2. The adaptive method is 4 times more efficient in the water-steel case, of similar efficiency in the air-water case and less efficient in the air-steel case. This can be explained by the stepsizes ratios in Table 2. The closer the multirate stepsizes ratios correspond to the adaptive ones, the better the performance of multirate in comparison with the adaptive method.

	Air-water	Air-steel	Water-steel
multirate ( $c_1 : c_2$ )	135 : 1	1 : 1	1 : 101
adaptive $u_0^1$	33.88 : 1	1.15 : 1	1 : 2.47
adaptive $u_0^2$	21.25 : 1	1.09 : 1	1 : 3.20

Table 2: Timestep ratios for the multirate and adaptive method (final grid) by materials.  $u_0^1$  is for the initial condition (25) and  $u_0^2$  is for (27).

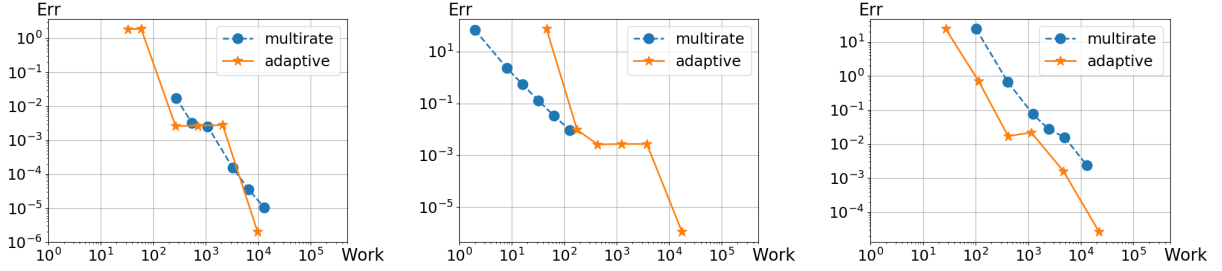


Figure 12: Left: Air-water. Centre: Air-steel. Right: Water-steel. DNWR work over error comparison for 2D test case using initial condition (25).

As second test case we consider the initial condition

$$u(x, y) = 800 \sin((x + 1)\pi)^2 \sin(y\pi). \quad (27)$$

Here, we have  $\mathbf{u}_\Gamma(0) = \mathbf{0}$  and thus skip the relative norm for the termination check (11). Results are shown in Figure 13 with stepsizes ratios in Table 2. In the air-steel case performance is approximately equal, whereas adaptive performance is about 4 resp. 25 times better in the air-water resp. water-steel case.

Overall we see that performance depends on the stepsizes ratios. This makes the adaptive method a more robust choice, since it automatically determines suitable stepsizes ratios, which vary for e.g., different initial conditions.

## 9 Summary and conclusions

We derived first and second order, multirate resp. time-adaptive DNWR methods for heterogeneous coupled heat equations. The optimal relaxation parameter  $\Theta_{opt}$  for WR is shown to be identical to the one for the basic DN iteration. We experimentally show how to adapt  $\Theta$  in the multirate case. The observed convergence rates using an analytical  $\Theta_{opt}$  for 1D implicit Euler

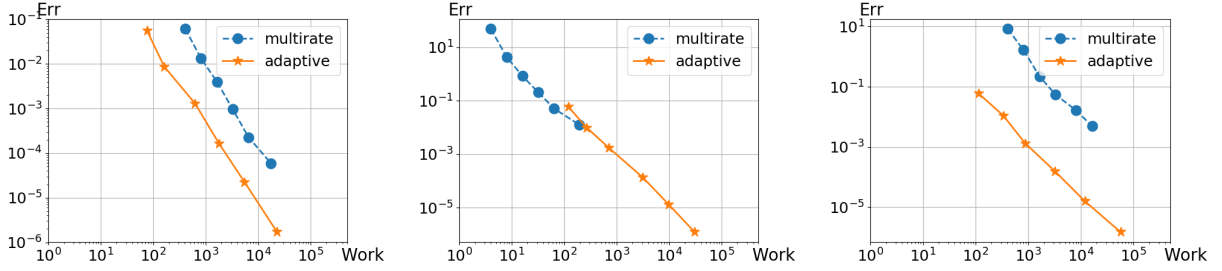


Figure 13: Left: Air-water. Centre: Air-steel. Right: Water-steel. DNWR work over error comparison for 2D test case using initial condition (27).

are shown to be very robust, yielding fast convergence rates for a second order method and 2D, for various material combinations and multirate settings on long time intervals.

The same tests for the related NNWR methods employing identical Dirichlet and Neumann subsolvers, using an analytical  $\Theta_{opt}$  for 1D implicit Euler, show a lack of robustness, possibly resulting in divergence.

The time-adaptive DNWR method is experimentally shown to be favorable over multirate, due ease of use and superior performance. The latter is due to the resulting stepsizes being more suitably chosen than those of the multirate solver. Overall, we obtain a fast, robust, time adaptive (on each domain), partitioned solver for unsteady conjugate heat transfer.

## References

- [1] C. ARÉVALO AND G. SÖDERLIND, *Grid-independent construction of multistep methods*, Journal of Computational Mathematics, 35 (2017), pp. 672–692.
- [2] A. BANKA, *Practical Applications of CFD in heat processing*, Heat Treating Progress., (2005).
- [3] P. BIRKEN, T. GLEIM, D. KUHLE, AND A. MEISTER, *Fast Solvers for Unsteady Thermal Fluid Structure Interaction*, Int. J. Numer. Meth. Fluids, 79(1) (2015), pp. 16–29.
- [4] P. BIRKEN AND A. MONGE, *Numerical Methods for Unsteady Thermal Fluid Structure Interaction*, In: Fluid-Structure Interaction. Modeling, Adaptive Discretisations and Solvers, Contributions in Mathematical and Computational Sciences, Springer, Berlin, (2017), pp. 129–168.
- [5] P. BIRKEN, K. QUINT, S. HARTMANN, AND A. MEISTER, *Choosing norms in adaptive FSI calculations*, PAMM, 10 (2010), pp. 555–556.
- [6] —, *A time-adaptive fluid-structure interaction method for thermal coupling*, Comp. Vis. in Science, 13(7) (2011), pp. 331–340.
- [7] S. BREMICKER-TRÜBELHORN AND S. ORTLEB, *On Multirate GARK Schemes with Adaptive Micro Step Sizes for Fluid-Structure Interaction: Order Conditions and Preservation of the Geometric Conservation Law*, Aerospace, 4(8) (2017).
- [8] J. BUCHLIN, *Convective Heat Transfer and Infrared Thermography*, J. Appl. Fluid Mech., 3 (2010), pp. 55–62.
- [9] P. CAUSIN, J. GERBEAU, AND F. NOBILE, *Added-mass effect in the design of partitioned algorithms for fluid-structure problems*, Comp. Meth. Appl. Mech. Eng., 194 (2005), pp. 4506–4527.

- [10] A. CRISTIANO, I. MALOSI, P. BLANCO, S. DEPARIS, AND A. QUARTERONI, *Algorithms for the partitioned solution of weakly coupled fluid models for cardiovascular flows*, Numer. Meth. Biomed. Eng., 27(12) (2011), pp. 2035–2057.
- [11] M. GANDER, L. HALPERN, C. JAPHET, AND V. MARTIN, *Advection diffusion problems with pure advection approximation in subregions*, in Domain Decomposition Methods in Science and Engineering XVI. Lecture Notes in Computer Science and Engineering, vol 50, pp. 239–246. Springer, Berlin., 2007.
- [12] M. GANDER, L. HALPERN, AND F. NATAF, *Optimized Schwarz waveform relaxation for the one dimensional wave equation*, SIAM J. Numer. Anal., 41(5) (2003), pp. 1643–1681.
- [13] M. GANDER, F. KWOK, AND B. MANDAL, *Dirichlet-Neumann and Neumann-Neumann waveform relaxation algorithms for parabolic problems*, ETNA, 45 (2016), pp. 424–456.
- [14] M. GANDER AND A. STUART, *Space-time continuous analysis of waveform relaxation for the heat equation*, SIAM J. Sci. Comput., 19(6) (1998), pp. 2014–2031.
- [15] E. GILADI AND H. KELLER, *Space-time domain decomposition for parabolic problems*, Numer. Math., 93 (2002), pp. 279–313.
- [16] M. GÖRTZ AND P. BIRKEN, *On the Convergence Rate of the Dirichlet-Neumann Iteration for Coupled Poisson Problems on Unstructured Grids*, in Finite Volumes for Complex Applications IX - Methods, Theoretical Aspects, Examples, R. Klöckorn, E. Keilegavlen, F. A. Radu, and J. Fuhrmann, eds., vol. 323 of Springer Proceedings in Mathematics & Statistics, Springer International Publishing, 2020, pp. 355–363.
- [17] E. HAIRER AND G. WANNER, *Solving Ordinary Differential Equations II - Stiff and Differential-Algebraic Problems*, Springer-Verlag, 1996.
- [18] U. HECK, U. FRITSCHING, AND B. K., *Fluid flow and heat transfer in gas jet quenching of a cylinder*, Int. J. Numer. Methods Heat Fluid Flow, 11 (2001), pp. 36–49.
- [19] M. HINDERKS AND R. RADESPIEL, *Investigation of Hypersonic Gap Flow of a Reentry Nosecap with Consideration of Fluid Structure Interaction*, AIAA Paper, 6 (2006), pp. 2708–3741.
- [20] J. JANSSEN AND S. VANDEWALLE, *Multigrid waveform relaxation on spatial finite element meshes: the discrete-time case*, SIAM Journal on Scientific Computing, 17 (1996), pp. 133–155.
- [21] D. KOWOLLIK, P. HORST, AND M. HAUPT, *Fluid-structure interaction analysis applied to thermal barrier coated cooled rocket thrust chambers with subsequent local investigation of delamination phenomena*, Progress in Propulsion Physics, 4 (2013), pp. 617–636.
- [22] D. KOWOLLIK, V. TINI, S. REESE, AND M. HAUPT, *3D fluid-structure interaction analysis of a typical liquid rocket engine cycle based on a novel viscoplastic damage model*, Int. J. Numer. Methods Engrg., 94 (2013), pp. 1165–1190.
- [23] F. KWOK, *Neumann-Neumann waveform relaxation for the time-dependent heat equation*, vol. 98, in Domain Decomposition in Science and Engineering XXI, J. Erhel, M.J. Gander, L. Halpern, G. Pichot, T. Sassi and O.B. Widlund, eds. Lect. Notes Comput. Sci. Eng., 2014.
- [24] E. LELARSMEE, A. RUEHLI, AND A. SANGIOVANNI-VINCENTELLI, *The waveform relaxation method for time-domain analysis of large scale integrated circuits*, IEEE Trans. Comput. Aided Des. Integr. Circuits Syst., 1(3) (1982), pp. 131–145.
- [25] B. MANDAL, *A Time-Dependent Dirichlet-Neumann Method for the Heat Equation*, vol. 98, in Domain Decomposition in Science and Engineering XXI, J. Erhel, M.J. Gander, L. Halpern, G. Pichot, T. Sassi and O.B. Widlund, eds. Lect. Notes Comput. Sci. Eng., 2014.

- [26] —, *Convergence analysis of substructuring Waveform Relaxation methods for space-time problems and their application to Optimal Control Problems*, PhD Thesis, 2014.
- [27] R. MEHTA, *Numerical Computation of Heat Transfer on Reentry Capsules at Mach 5*, AIAA-Paper, 178 (2005).
- [28] P. MEISRIMEL, *Adaptive time-integration for goal-oriented and coupled problems*, PhD Thesis, Lund University, 2021.
- [29] A. MONGE, *Partitioned methods for time-dependent thermal fluid-structure interaction*, PhD Thesis, Lund University, 2018.
- [30] A. MONGE AND P. BIRKEN, *On the convergence rate of the Dirichlet-Neumann iteration for unsteady thermal fluid-structure interaction*, Computational Mechanics, 62(3) (2018), pp. 525–541.
- [31] —, *A multirate Neumann-Neumann waveform relaxation method for heterogeneous coupled heat equations*, SIAM J. Sci Comput., 41 (2019), pp. S86–S105.
- [32] A. MONGE AND P. BIRKEN, *A time-adaptive Dirichlet-Neumann waveform relaxation method for coupled heterogeneous heat equations*, PAMM, 19 (2019), pp. 2–3.
- [33] —, *Towards a Time Adaptive Neumann-Neumann Waveform Relaxation Method for Thermal Fluid-Structure Interaction*, in Domain Decomposition Methods in Science and Engineering XXV, O. Haynes, R., MacLachlan, S., Cai, X.-C., Halpern, L., Kim, H.H., Klawonn, A., Widlund, ed., vol. 138 of Lecture Notes in Computational Science and Engineering, Springer, 2020, pp. 466–473.
- [34] A. M. PETER MEISRIMEL. <https://github.com/PeterMeisrimel/DNWR>. Accessed: June 30, 2020.
- [35] B. RÜTH, B. UECKERMAN, M. MEHL, P. BIRKEN, A. MONGE, AND H.-J. BUNGARTZ, *Int. J. Num. Meth. Eng.*, (2020), pp. 1–23.
- [36] G. SÖDERLIND AND L. WANG, *Adaptive time-stepping and computational stability*, J. Comp. Appl. Math., 185 (2006), pp. 225–243.
- [37] P. STRATTON, I. SHEDLETSKY, AND M. LEE, *Gas Quenching with Helium*, Solid State Phenomena, 118 (2006), pp. 221–226.
- [38] A. TOSELLI AND O. WIDLUND, *Domain Decomposition Methods - Algorithms and Theory*, Springer, 2004.
- [39] E. VAN BRUMMELEN, *Partitioned iterative solution methods for fluid-structure interaction*, International Journal for Numerical Methods in Fluids, 65(1-3) (2011), pp. 3–27.